Laura Rojas Rojas

Fabrication techniques for developing a functional microfluidic glass device suitable for detection in optical spectroscopy system

Master's Thesis
in Physics
December 3, 2012

UNIVERSITY OF JYVÄSKYLÄ
DEPARTMENT OF PHYSICS

Jyväskylä

Author: Laura Rojas Rojas

Title: Fabrication techniques for developing a functional microfluidic glass device suitable for detection in optical spectroscopy system

Supervisor: Andreas Johansson

Degree: Master of Science

Department: Department of Physics

Project: Master's Thesis in Physics

Page count: 55

Abstract:

Microfluidic devices offer the chance to manipulate and analyze fluids including bioassays and chemical reactions. In this study, a method to develop a microfluidic analysis system is proposed for detection of nanotubes by a Raman acquisition setup.

Microchannels where fabricated in sodalime glass substrate by MeV ion beam lithography or electron beam lithography and wet etching. Fusion bonding (550 °C) was used to seal the microchannels. As a result a prototype microfluidic device with 1.6 μm deep channel that exhibit efficient sealing and suitable channel geometry was obtained. The microfluidic device was tested in a Raman spectroscopy detection system and the collected spectra showed the presence of carbon nanotubes within the channel with clear RBM and G-band peaks.

By this approach a practical and simple fabrication technique for microfluidic devices combined with Raman spectroscopy was done. This device can be enhanced to perform concentration maps within the channel and further research can focus on performing steady constant fluid flow inside the channel.

Keywords: Microfluidics, thermal bonding, lithography, wet etching, Raman spectroscopy

Preface

From October 2011 until September 2012 I had the opportunity to work on a Master's thesis research project at the University of Jyväskylä. The project was conducted at the Department of Physics in the Pelletron laboratory and at the Nanoscience Center. To work in this project and have studied in the University of Jyväskylä exceeded my expectations, and for that I am most grateful.

I offer my sincerest gratitude to my supervisor Dr. Andreas Johansson for his advice throughout the project. I really appreciate all the guidance he gave me while performing the experimental procedures and the patience he showed me while the writing the thesis. I am also grateful for the motivation he gave me when working.

As well, I would like to thank the members of the Pelletron Accelerator group for their help and collaboration during the experimental work. Special acknowledgements for all the people of the Nanoscience Center, thank you for your assistance in training me into using the equipment and for your patience and kindness. It was truly a pleasure to work beside all of you.

I have special appreciation towards the E2NHANCE project and Instituto Tecnológico de Costa Rica (ITCR) for enabling this mobility program and providing financial support for me during the duration of my studies.

Last but not least, I owe my deepest gratitude to my family and friends who helped me, guided me, and support me along the duration of my studies in Finland. Through this process your support and encouragement, even in difficult times, were always motivating me to work harder and do my best. The love and guidance you gave me will be a part of me as a great memory. This document would not have been possible without you. Thank you!

Contents

1 Introduction

Microfluidics incorporates the fabrication techniques and analytical methods that are related with fluid manipulation on the micrometer scale [1]. The observation and analysis of systems in this scale results in great academic and commercial potential that include valuable applications in biochemical assay development, biosensors and chemical synthesis applications [2, 3]. Microfluidic devices have been used for sorting and trapping particles, and identification of molecular interactions by optical and electrochemical methods [4–7].

Common fabrication techniques of microfluidic devices include lithography procedures in combination with wet etching on polymer or silicon substrates [2, 8, 9]. Accessible techniques, reproducible procedures and fast fabrication methods are desired attributes for the production of microfluidic devices [10]. This research focuses on the fabrication procedures to develop a functional microfluidic device on sodalime glass for the detection and analysis of bio-chemical compounds in a Raman spectroscopy system.

To develop a microfluidic channel on sodalime glass, MeV ion beam lithography and electron beam lithography techniques are used. Their underlying characteristics, such as the exposure parameters and mask layer deposition are studied. Besides, to etch the microchannel on sodalime glass, the etchant concentration and the etching time are examined for exposed and unexposed sodalime glass. In addition, thermal bonding procedures are performed. The optimal bonding temperature is studied and the addition of external pressure is explored to achieve bonding of two pieces of glass to enclose the microfluidic channel and obtain a functional microfluidic device.

2 Fabrication techniques of glass microfluidic devices

Fabrication techniques of microfluidic devices incorporates patterning methods, wet etching steps and bonding of the substrates. Moreover, microfluidics includes many possibilities of analysis and synthesis of compounds and provides a wide variety of applications. This chapter provides a general description of the available fabrication methods and a brief introduction towards applications of glass microfluidic devices.

2.1 General description of fabrication techniques

There are several parameters that need to be examined to fabricate microfluidic devices. The fundamental parameters are the chemical composition of the substrate, the patterning method, enclosing the microchannel and the addition of external connections either for fluid movement or for performing detection. These parameters will determine the characteristics and performance of the resulting device [3, 10].
The chemical composition of the substrate determines its properties. Mechanical, electrical, optical and thermal properties should be considered to select an appropriate substrate to be compatible with the analyte and to adjust with the subsequent detection system. Polymeric materials, silicon and glass are widely used as substrates for microfluidic devices.
Polydimethylsiloxane (PDMS) and Poly(methylmethacrylate) (PMMA) are commonly used because of their versatility in surface modification [11, 12]. These substrates are optically transparent and present good electrical and mechanical properties. Also, silicon and glass can be utilized as a substrate for microfluidic devices. These are preferred when stable and rigid properties are needed.
Glass substrates come of interest when the system has to operate in high temperature or high pressure. Also, using glass as a substrate is beneficial for analysis in

optical methods [10]. Glass allows electrokinetically driven fluid flow, it is highly resistant to organic and it is biocompatible.

It is possible to perform combinations between the substrates. When two different substrates are used, the properties of the substrates have to be examined. For instance, the expansion coefficient, the conductivity and their response to mechanical stress are different in each type material. Also the analyte compatibility with the microchannel has to be considered [13]. Using a polymer intermediate layer sacrifies homogeneity

Once the substrate has been chosen, the method for lithographic patterning should be determined. Electron beam lithography (EBL) [8], embossing, injection molding, laser ablation [1], and photolithography [2, 9] are widely used. Depending on the lithographic method certain steps are necessary to obtain the desired pattern in the substrate. For instance, EBL requires sensitive resist deposition on the substrates surface, photolithography requires careful mask placement and injection molding of polymers involves precise curing of the substrate. The lithography step is usually followed by chemical wet etching in HF or buffered etch solvent.

After the channel has been created or transferred to the substrate it is necessary to enclose it in order to seal the channel to obtain fluid flow. Several bonding techniques that can be employed are thermal bonding or direct bonding, anodic bonding, and assisted bonding by addition of intermediate layers between the substrates [10–12]. Strict cleaning protocols have to be followed in relationship to the chosen substrate to achieve successful bonding.

2.2 Glass characteristics and applications for microfluidic devices

Common glasses are solid materials mainly composed of silicon dioxide (SiO_2). Glass materials contain other oxides in their composition. Boron oxide, sodium oxide, calcium oxide and magnesium oxide can be found in different proportions in the structure of glass.

Silicon dioxide has a three dimensional crystal-like structure made up of SiO_4 tetra-

hedra. The structure of glass varies from the ordered tetrahedra because of the oxides present within its chemical composition. Glass presents an amorphous crystalline structure in which there is no long-range order as in a crystal.

The general properties of glass include rigidness, chemical inertness and good spectral transmission at the visible wavelengths. These properties are modified by the proportions of the oxides in the composition of glass. Different mechanical, thermal and optical properties are obtained depending on the amount of oxides.

When glass contains about 12% boron trioxide, the glass is called borosilicate glass. These glasses have low thermal expansion coefficients. Borosilicate glass is often used for kitchenware and laboratory glassware. Sodalime glass has high sodium oxide composition, about 13% in its structure. This glass is used for windows and containers such as bottles. Sodalime glass can be considered a relatively low cost material and it is commercially available by many manufacturers.

Glass microfluidic devices are versatile tools for a wide variety of assays. Microchannels within glass may be produced with two different cross-sectional geometries. One has a semicircular profile and the other has a rectangular profile. The application of the device will depend on its configuration, for example the semicircular bottom can be used to produce micro-lenses [9]. Applications of glass microfluidic devices include immunological assays or analysis of single cell components, also DNA analysis, cell lysis by a flow cytometer [14], and proteonomics.

The optical characteristics of glass give it a large application potential where optical methods are used for modification or detection. For example, Schafer et al. [15] use optical fibers integrated in a microfluidic chip as a cell counter. Optical detection is the most used among researchers because of its high sensitivity and ease of implementation. Also, glass microfluidic devices can be used for chemically driven reactions [16], in capillary electrophoresis [17] and as a chromatography chip [18].

Laser induced fluorescence presents a good option to perform detection in glass devices or combined glass devices. Chou et al. [6] uses 500 nm channels in fused silica for detection of two protein interaction in a very rapid way by using laser induced fluorescence in a simple channel cap with a glass coverslip. And Wang et al.

[5] use a long 25 μm deep glass channel to determine 5 β-casomorphins, proving that this method is sensitive and reliable for peptide detection methods. Also, ph gradients in glass have been performed by functionalizing a polymer membrane inside the channel by Cheng and Chang [19].

Spectroscopic measurements from fluorescence systems offer high sensitivity with the only drawback of handling the autofluorescence from the chip. Raman spectroscopy is also utilized for analytical applications because it can give a spectrum of the analyte in the aqueous phase [4, 7].

Glass microfluidic devices are also used with electrochemical detection methods [18] Electrochemical methods are detection systems based on bio-molecular recognition performed through selective analysis of chemical reactions. Besides recognition, this method involves signal modification, which relies in transforming the identified reaction into an electrical signal. Subsequently this signal has to be interpreted.Yi et al. [20] present recent developments in electrochemical detection methods for microfluidic applications.

Kinetic studies involve pressure driven flow or electrokinetic driven flow. Glass is suitable for these studies because it is very robust and most likely it will not deform under high pressure assays. For example reactions between two chemicals can be studied by using a simple T configuration [2, 21]. Since glass allows application of varying electric fields, a preconcentrator has been used to detect liposomes in glass microchannels by making a photopolymerized membrane inside [22]. When using hydrodynamic methods, it is possible to divide, count or sort micro particles. Also when two immiscible substances are combined, the creation of droplets can be performed [21].

2.3 MeV ion beam lithography

2.3.1 Ion matter interactions

Energetic ions interact with the atoms that compose a material by nuclear and electronic scattering. Nuclear scattering and nuclear energy loss is related with the interactions between the incident ion nucleus and the nuclei of the target material atoms. Electronic energy loss takes place when the projectile ion interacts with the electrons. As a consequence of these interactions, the ions lose their energy by transferring it into the target material.

Ions travel through the target until their energy is completely absorbed. The energy loss per unit of length of a non relativistic ion in a trajectory is composed of

$$\frac{dE}{dx} = \left(\frac{dE}{dx}\right)_{\text{nuclear}} + \left(\frac{dE}{dx}\right)_{\text{electronic}} \tag{2.1}$$

where $\frac{dE}{dx}$ is known as the stopping force.

The range or penetration depth is the distance of an ion inside a solid due to complete energy loss. The penetration depth of the ions depends on their initial kinetic energy and on the total stopping force, see eqn. 2.1. For 6.8 MeV 16 O ions the theoretical projected range can be estimated by using the Stopping and Range of Ions in Matter (SRIM) [23]. A SRIM simulation for the projected range in sodalime glass with composition in mass percent of O 46.52%, Si 34.03%, Na 11.14%, Ca 5.83%, Mg 1.18% and Al 1.31%, yields approximately 4.94 μm.

In addition SRIM allows the estimation of the ionization or electronic energy loss [23]. Figure 2.1 shows the ionization as a function of the target depth. The electronic stopping remains constant from 0 μm to 2 μm, and then decreases linearly to zero. Also fig. 2.1 shows the stopped ions. The ions are stopped close to 5 μm.

Projectile ions incident on a target modify the atomic bonds in the solid. Depending on the composition of the substrate and the initial energy of the ion, the atomic bonds in the target can either be broken or new bonds can be formed by cross-linking [24]. When the bonds are broken, the structure gets damaged and therefore

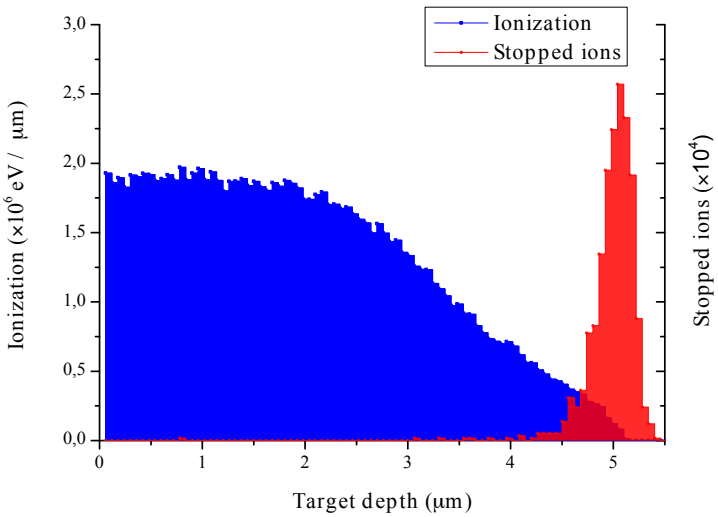

Figure 2.1: The ionization for 6.8 MeV ^{16}O ions as a function of the depth and their corresponding range in a sodalime target.

it is susceptible to dissolution. The damaged area can be removed selectively to produce a lithographic pattern into several substrates [25–27].

Silica and glass have been used as a substrate to make a lithographic pattern by direct exposure. For instance, Momota et al. [28] exposed Si substrate to an Argon beam and Puttaraksa et al. [27] used $^{16}O^{3+}$ ions to write patterns in silica substrate. The composition of glass and silica is very similar hence one may anticipate the procedure can be extended to develop a microfluidic channel in a glass substrate. This method involves exposure of the substrate to the ion beam without a mask followed by etching of the exposed area, previously described by Puttaraksa et al. [27].

2.3.2 The ion beam lithography system

The Accelerator Laboratory of the University of Jyväskylä, Finland, is equipped with a Tandem Pelletron accelerator and a Programmable Proximity Aperture Lithography (PPAL) system which is used as a lithography system, previously described by Gorelick [29] and Puttaraksa [21]. Fig. 2.2 depicts a schematic of the system.

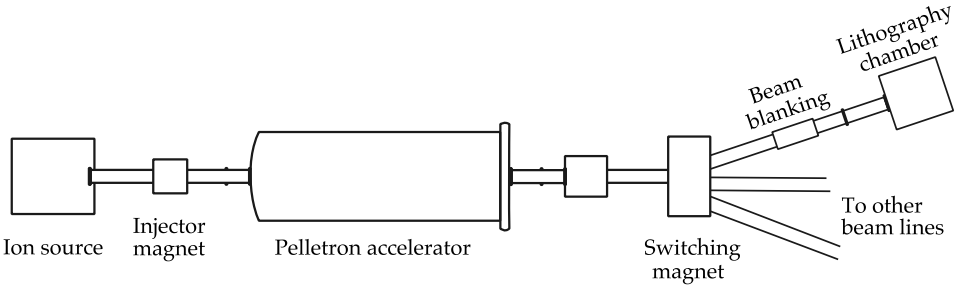

Figure 2.2: Layout of the ion beam lithography accelerator line. The injector line begins with a sputtering ion source that is connected to the Pelletron accelerator. The ion beam is directed towards the lithography chamber by a switching magnet.

The injector beam line starts with a Source of Negative Ions by Cesium Sputtering (SNICS). In the ion sputtering source, a cathode made of copper is loaded with powder containing the element that will be accelerated. By sputtering the cathode with cesium, the negative ions are extracted from the target. Then the desired ions are selctd by an injector magnet into the acceleration tank.

After the negative ions enter the accelerator tank, they are accelerated twice inside it. First to a positive potential in the middle of the tank and subsequently to ground potential at the end of the chamber. After passing through the first acceleration stage, the ions go through a stripping canal filled with low pressure nitrogen gas in which their electrons are removed. This process yields positively charged stripped ions with several charge states.

These positive ions are then accelerated down to ground potential in a second accelerator stage. Then, by using a switching magnet the ion beam is directed into the line that leads to the lithography chamber. In addition, the charge state is selected by means of a switching magnet.

Before the beam reaches the lithography chamber, there is an electrostatic beam blanker. The beam blanker allows the beam to be turned on or off. This is controlled by computer.

At the end of the beam line there is a lithography chamber. Figure 2.3 gives a representation of the components within the chamber. The lithography chamber contains a sample holder, two L-shaped tantalum (Ta) blades placed in aluminum (Al) blocks

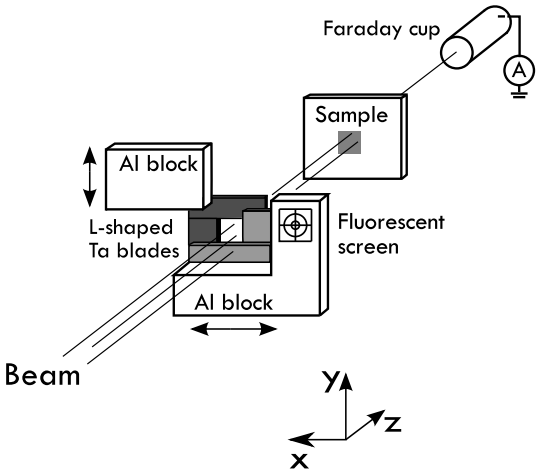

Figure 2.3: Schematic representation of the PPAL system inside the lithography chamber. After Puttaraksa et al. [30].

that restrict the size of the beam to a rectangular shape. Also in the chamber there is a fluorescent screen for viewing the beam, and a Faraday cup for measuring the beam current that reaches the chamber. Sample holder stage movements, the opening aperture size and the time of exposure are computer controlled by a LabView program [26, 27].

The Ta blades in the PPAL system shape the size of the ion beam. By controlling the size of the opening between the blades and the position of the sample, rectangular patters can be irradiated into the substrates [21, 29]. A succession of rectangles can be used to obtain a wide variety of shapes. These rectangles are written by means of a computer program that stores their coordinates and transmits them to the PPAL system. To pattern a channel, consecutive rectangular exposures are needed.

The exposure parameters that can be selected are ion species, energy, and fluence. Ion species are selected by using a desired material in the sputtering cathode. The energy of the ions will be selected by the accelerator terminal voltage. Ion fluence is the amount of ions per unit of area (ions cm^{-2}). In the PPAL system, the amount of ions that reach the sample will be restricted by the opening area in the L-shaped blades, see fig. 2.3.

2.4 Electron beam lithography on glass

A common lithography technique is to use an electron beam to write over an electron sensitive layer. The beam is focused and then it scans through the surface of the sample exposing selected areas of the sensitive layer. The exposed or unexposed regions can be removed by developing it in a solvent.

Electron beam lithography can be used to pattern indirectly a glass substrate. Several stages are required to transfer a lithography pattern in a glass substrate. Rodriguez et al. [8] have reported the procedure as: 1) deposition of a metal layer or mask layer and an appropriate resist; 2) exposure and developing of the resist; 3) wet etching through the exposed metal layer; 4) wet etching of the glass through the metal etch mask; and 5) removal of the metal mask.

To pattern a glass substrate by electron beam lithography the presence of an etchting-resistant mask and an electron sensitive film is required. Frequently for a glass substrate Cr and Au are used. A thin film of Cr is used on the surface of glass as an adhesion layer for the Au layer. And Au is used as the protective layer because it is chemically inert to a wide variety of etchants [31].

The resist used in electron beam lithography is typically a thin layer of an organic polymeric material. Classic examples are poly(methyl methacrylate) PMMA and poly(butene sulfone) PBS. The chemical composition of the resist will change when it is exposed. Their molecular chains can be broken into short chains making them susceptible for removal in a developer. If the polymer is made of short chains, they can be joined when exposed. This makes the exposed sections insoluble to a developer.

Also, there have been studies regarding direct exposure of inorganic resists. For example, Beaumont et al. [32] made direct-writing by EBL in silicon dioxide to create patterns of different depths by changing the doses (C cm^{-2}) and using HF as the etchant. A similar procedure could be adopted as a possibility to perform direct lithography on glass with which the presence of a mask on the surface of the glass will be avoided.

2.5 Wet etching of glass in hydrofluoric acid

Glass is dissolved in hydrofluoric acid because the acidic solution breaks the siloxane bonds (Si−O−Si) within the glass structure [33]. Etching occurs by the diffusion of soluble ions across the glass-acid solution interface. Through wet etching the superficial layers of the substrate will be removed, therefore the morphology of the surface will change [34, 35]. The thickness of the etching layer removed as a function of time is the etch rate ($\mu m/s$). The etch rate depends on the concentration of the etchant and the composition of the glass.

Sodalime glass is a multicomponent glass, as described in section 2.2. It has a small fraction of oxides within its composition. When etching a multicomponent glass with HF, the siloxane bonds are broken and the products of the oxides are released into the solution. These products will form precipitates at the glass-acid interface which are insoluble in HF. The addition of hydrochloric acid (HCl) to the etching solution will remove the insoluble products like CaF_2 and MgF_2 [34]. To improve the reaction, the solution could be agitated which will also reduce the build up of insoluble debris on the surface.

HF etching of glass often leads to irregular shapes and an increase on the surface roughness. Also, HF etching is isotropic which leads to a semicircular etch profile. The resulting roughness of the etched glass structure and its profile strongly depends on the HF concentration and the etching time [36].

The HF concentration and the etching time used to etch the pattern on a glass substrate are dependent on the lithographic technique. For instance, when indirect lithography is used, etching has to be performed through a mask. Therefore, concentration of the HF and the etching time have to be carefully controlled in order to prevent mask deterioration and adequate pattern transfer [35, 36].

Several characteristics about the masking layers have been studied to optimize the adhesion of the mask layer to the substrate. For example, Mourzina et al. [37] reports that there is no difference in using evaporated metal etch masks and sputtered metal films as sacrificial layers in glass etch process. These authors obtained 6 - 16 μm deep

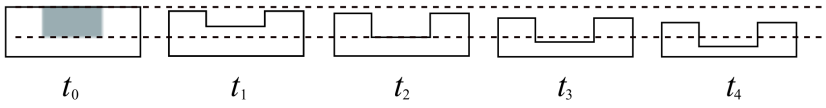

Figure 2.4: Proposed model for behavior of etching of exposed and unexposed sodalime glass. The model shows different cross-sections of the glass when etching time increases, $t_1 < t_2 < t_3 < t_4$. In t_0 glass hasn't been etched and the shaded gray section represents the penetration depth of the ions. t_i shows the expected profile of the glass after etching in HF.

channels in pyrex glass. A through etched hole on glass has been performed by Tay et al. [38] using a 50 nm of Cr, 1 μm of Au and a photoresist mask, these combination of layers are adequate to protect the glass substrate from a mixed etching solution containing HF:HCl.

Iliescu et al. [35] provides several options of effective mask layers for deep wet etching of Pyrex glass. For example, photoresists, amorphous silicon, Cr/Cu, among others layers are compared and discussed. Also, it is shown that the defects of the etched pattern depend on the design of the masking layer.

The etching rate and resulting surface roughness vary if glass has been irradiated. Regular behavior of unexposed glass in HF establishes that as the etching time increases so does the erosion of the glass. The expected behavior for etching of exposed glass relies in the property that exposed glass is removed in faster etch rate once in contact with the acid. Irradiation using an ion beam into the glass substrate induces damage to the network and therefore the HF dissolves locally this section faster [39].

Once the exposed area is removed, the acid continues to etch uniformly through the glass, etching away layer after layer of the same profile. In principle this allows the original morphology to be maintained on the surface. Fig. 2.4 shows a proposed model of the etching behavior of glass.

First the irradiation of the surface damages a specific section of the glass substrate. The exposed area is shown in fig. 2.4 as a shaded grey section and denoted by t_0. This interaction area could be partially or entirely removed. When the damaged area is completely removed, the threshold value is reached at t_2. The threshold

will represent the maximum etch depth that could be achieved corresponding to damaged made.

It is in the limit when all the exposed area is removed and less unexposed area is withdrawn by chemical wet etching. This etching time is crucial because it will provide valuable information of how to achieve different depths in the glass substrate. If the etching time is less than t_2, the exposed area is partially removed. And if the etching time is larger than the threshold value, for example in t_3 and t_4 of fig. 2.4, the surface profile is maintained but more unexposed glass is removed. This study suggests that when the threshold value is reached the surface profile should be maintained because the etching rate will be constant.

2.6 Direct thermal bonding

Bonding of glass can be achieved by placing two pieces together at elevated temperature. This procedure is often called thermal bonding or fusion bonding. For microfluidic devices, one of the to-be-bonded pieces contains a previously etched microchannel and the other is a plain slide.

Direct bonding is often performed when both pieces have the same material composition, however they can differ in thickness. For example a microscope glass slide and a coverslip. Also, combinations of materials as polymers and glass are in use. When two materials of different composition are going to be bonded their expansion coefficients would be necessary parameters to explore to avoid breaking.

The desired attributes of a bonding procedure are high bond strength, and robustness against flaws. Also it is relevant to prevent bond degradation and reduce manufacturing time. Some parameters to be considered during the procedure are the temperature, and addition or removal of pressure [40].

The chosen temperature is dictated by composition of the glass and the design of the chip. These characteristics are unique to the chip in hand, for sodalime glass transition temperature is found to be between 560 °C and 580 °C [13]. If the melting temperature of glass is exceeded, the microchannel can collapse because of melting.

And if the temperature is too low, strong bonding will not occur.

Various options for direct bonding of glass have been explored to optimize the procedure at different temperatures, for example Jia et al. [16] made successful bonding of glass at room temperature, while Lin and Kuo [41] and Mao and Han [42] used 580° C and 550° C respectively. The most important factor to consider is the cleanness of the substrates [43].

Good cleaning procedures to remove solid particles and organic contaminants include using acetone, isopropanol (IPA), and acidic solutions. Lin and Kuo [41] use piranha solution 3 H_2O_2 : H_2O ratio to clean borosilicate glass, Chen et al. [43] report a combination of ammonium hydroxide and piranha solution NH_4OH - H_2O_2 - H_2O with a 0.5:1:5 ratio as the optimal cleaning solution for soda lime glass, or HNO_3 can be used [10]. Also ultrasonic cleaning steps in intervals of 3 min in deionized water (DI water) are beneficial [44].

In addition to the cleaning procedures, several authors have reported that the surface should be activated by exposing -OH groups [45]. These groups will improve the adhesion because they are highly energetic. Another possibility is to activate the surface with calcium (II) acetate or use intermediate films to improve the adhesion [46].

Moreover, when direct bonding is employed, other considerations regarding the holes for external connections, the composition and the thickness of the glass samples should be considered. To avoid stressing the samples one of the glass pieces should have holes made for external connections prior to bonding. If the holes are made after bonding there is a risk of damaging the microfluidic chip. Small debris from drilling may also block the channel preventing fluid flow [13].

3 Raman spectroscopy of carbon nanotubes

Carbon nanotubes exhibit different properties related to their configuration. Depending on their arrangement different applications can be obtained. The characterization of carbon nanotubes provides valuable information about their properties. Raman spectroscopy offers the possibility to study the structure of carbon nanotubes by analyzing their spectra. A general overview and background information about carbon nanotubes is given in the following chapter.

3.1 Carbon nanotubes

A planar lattice of carbon atoms arranged as hexagonal rings compose a graphene sheet, see fig. 3.1. When this sheet rolls itself as a cylindrical tube it is possible to obtain carbon nanotubes [47]. A single-walled carbon nanotube (SWNT) is made so that the structure becomes one-dimensional, there would be only one layer of graphene forming the tube. When these layers are concentric one after the other, multi-walled carbon nanotubes (MWNT) are obtained.
The structure of a nanotube is characterized by the chiral vector $\vec{c}$ in eqn. 3.1, and the chiral angle θ in eqn. 3.2

$$\vec{c} = n\vec{a}_1 + m\vec{a}_2 \tag{3.1}$$

$$\tan\theta = \sqrt{3}\frac{n}{2m+n} \tag{3.2}$$

where n and m are integer numbers that represent the different structures that the nanotubes originate. The geometry and symmetry of the nanotubes is defined by these two values. The basis vectors, $\vec{a}_1$ and $\vec{a}_2$ are of length 2.46 Å. When $n = m$ the nanotubes are called armchair nanotubes. If $m = 0$ zigzag nanotubes are obtained [47]. The arrangement of these tubes is visualized in fig. 3.1.

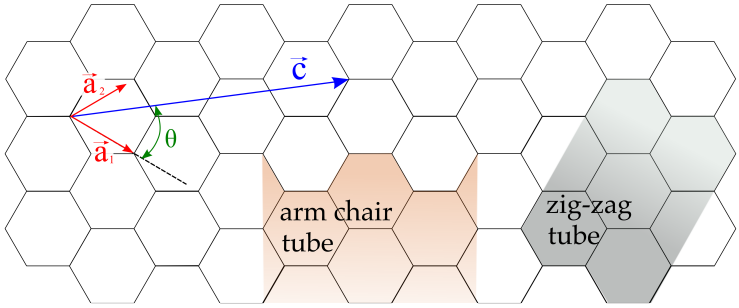

Figure 3.1: Scheme of a graphene sheet. Chiral vector and angle are denoted by $\vec{c}$ and θ respectively. In orange there is the model for a armchair nanotube and in grey the model for a zigzag nanotube.

The diameter d, corresponding to the nanotube can be obtained by the relationship of length of the basis vectors and the pair of integers m, n that uniquely define the tube:

$$d = \frac{a}{\pi}\sqrt{n^2 + nm + m^2}. \tag{3.3}$$

Different properties arise from the cylindrical structure of carbon nanotubes, for example they exhibit very high current densities (1×10^{10} A cm^{-2}) and high thermal conductivity [48]. These properties are dependent on the diameter of the tube, their wrapping and morphology [47]. For instance, armchair carbon nanotubes are metallic and have higher tensile strength than zigzag nanotubes. Mechanical properties are influenced by the chirality or rotation of the tube.

One fabrication technique of carbon nanotubes is the arc discharge method [49]. This technique uses an arc ignited between two high-purity graphite electrodes that work as an anode and a cathode. Both electrodes are in a gaseous helium atmosphere. The arc ignition causes the graphite to evaporate and the evaporated material deposits on the cathode. This deposit contains the carbon nanotubes and other carbon particles [47]. By this method multimorphology nanotubes are produced.

Laser ablation uses a pulse of laser light on a target carbon surface and a metal catalyst such as Co or Ni. The target is placed in a stream of helium gas. The evaporated material is condensed and deposited on a collector. The incorporation of a metal

catalysts in the target enhances the formation of SWNT [47]. Arc discharge and laser ablation rely on powdered samples that contain nanotubes in a mixture, therefore it is not possible to perform controlled synthesis and obtain ordered nanotube structures. These two methods are related with the condensation of carbon atoms generated by evaporation of solid carbon [50].

Another technique to synthesize carbon nanotubes is chemical vapor deposition (CVD) [51]. This technique offers arrays of controlled diameter and length carbon nanotubes [47]. The final purity of the material is high [50]. In addition this technique is important in industry to produce SWNT [50].

CVD produces carbon nanotubes by the decomposition of a volatile compound of carbon, catalyzed by metallic nanoparticles. The carbon containing gas is flowing and therefore replaced continuously. By regulating the carbon gas pressure, the size and diameter of the output nanotubes can be controlled.

High pressure catalytic decomposition of carbon monoxide (HipCO) uses carbon monoxide gas and a catalytic $Fe(CO)_5$ material. The CO gas is heated. Then as it flows it is mixed with $FeCO_5$. This is a method for the preparation of SWNTs using high-pressure CO as the carbon source [50].

3.2 Raman spectroscopy

One way for characterizing carbon nanotubes is to use their Raman spectra. The energy and the pathway of photons change due to elastic and inelastic interactions with matter. Raman scattering occurs when the interaction is inelastic, therefore there is a decrease on the energy.

Absorption of a phonon can create an electron hole pair inside a material when there is an absorption of a photon. The electron-hole pair scatters by the emission of a phonon. This phonon recombines within the material and a scattered photon is emitted. The change in the frequency of the emitted photons is called the Raman effect. The Raman effect offers information about the vibrational, rotational and other frequency transitions in the molecules.

Raman spectroscopy uses monochromatic light of a known frequency focused on the sample. The incident photons are absorbed and reemitted. A spectrum can be produced from the intensity distribution of the emitted photons. In Raman spectroscopy the vibrational frequencies are measured as a shift of the incident beam frequency.

Raman spectrum is very sensitive to the structure of the carbon nanotube. The coefficients m and n in eqn. 3.3 will resolve different Raman shifts, so each tube with different diameter will exhibit a distinct spectrum.

There are three main peaks that can be found in a Raman spectrum of carbon nanotubes. These peaks have been widely identified [52, 53]. The radial breathing mode (RBM) lies in a frequency of 100-400 cm^{-1} and it is related to the oscillations of the diameter of the tube. RBM is useful in the identification of the nanotube's diameter from the absorption spectra [52].

According to eqn. 3.4, by measuring the RBM frequency ν_{RBM} in cm^{-1}, the diameter d in nm of the nanotubes can be found. Consequently this will provide information about the structural parameters n, m.

$$\nu_{RBM} = \frac{223.5}{d} + 12.5 \tag{3.4}$$

At a frequency of 1300-1400 cm^{-1} there is a double-resonance process, and it is called a D-band vibration. Then, the G-band is related with the electronic properties of carbon nanotubes and it comes from the vibrations of the sp^2 carbon materials. The range of frequencies for the G-band are between 1500-1605 cm^{-1}. There are differences between the shape and the position of these peaks according to the electronic and geometrical structure properties of the carbon nanotube [52].

Raman spectroscopy can be used for mapping spatial concentrations of carbon nanotubes or to probe inter diffusion [7]. Since glass gives a relatively weak Raman spectrum, it represents a good measuring substrate. Also, the SWNT made by HipCO process exhibit small diameters and are usually favored for spectroscopy studies because they sharp and well-separated peaks [52].

4 Experimental Techniques

The procedures to obtain a microfluidic channel enclosed in sodalime glass are discussed in this chapter. Two distinct lithographic techniques for patterning were used: MeV ion beam lithography (section 4.3) and electron beam lithography (section 4.4) in combination with wet etching. In addition, thermal bonding techniques are described. Finally, this chapter contains the steps to acquire a Raman spectrum of carbon nanotubes.

4.1 Substrates

Microscope slides and coverslips (Menzel-Glaser) of sodalime glass were used as the substrate for this study. The microscope slides have dimension of 26 $\times$ 76 mm and 1.0 mm thick, and coverslips have dimension of 24 $\times$ 40 mm and 0.16 - 0.19 mm thick. The chemical composition is SiO_2 72.2%, Na_2O 14.3%, CaO 6.4%, MgO 4.3%, K_2O 1.2%, Al_2O_3 1.2%, Fe_2O_3 0.03% and SO_3 0.3% according to manufacturer.
The microscope slides and coverslips were cut in squares of approximate 1 cm^2. Then, they were cleaned in acetone and IPA and stored for further processing. Throughout the study lithographic patterns were fabricated in the 1 mm thick substrates.

4.2 Examination on wet etching

For wet etching of glass, hydrofluoric acid (J.T. Baker) 38% and hydrochloric acid (J.T. Baker) 37-38% were used. Both chemical solutions were diluted in deionized water. The concentration is reported in volume per volume (v/v). Two different solutions were used in this study. One was a 4% v/v HF and the other was a mixture of 6% v/v HF and 0.5% v/v HCl with a 12:1 ratio.

The sodalime glass substrates were selectively masked with a polymer derived adhesive (electric tape). Then the samples were submerged in both of the HF solutions at room temperature T=20 °C by gradually increasing their immersion time. After the samples were etched, they were rinsed in DI water for 5 min. Then the adhesive mask was removed and the resulting etch depth was measured with stylus profilometer (KLA-Tencor P-15 Profiler).

4.3 MeV ion beam lithography

Prior to irradiation of the samples, the sodalime glass squares were cleaned in hot acetone, rinsed in IPA, and finally dried by nitrogen gas at room temperature. Once the substrates were cleaned, the 1.7 MV Pelletron accelerator was used to irradiate the samples by using a 6.8 MeV $^{16}O^{3+}$ ions.
The beam was obtained from a sputter cathode composed of aluminum oxide Al_2O_3. The beam is then accelerated and directed into the lithography chamber, see fig. 2.2. The current inside the chamber was measured with Faraday cup before doing the irradiation of the samples.

4.3.1 Direct writing on glass

Figure 4.1 gives an overview of the steps utilized to study the etching behavior of exposed sodalime glass. Sodalime glass samples were exposed to $^{16}O^{3+}$ ion beam. The patterns to be exposed were 8 squares of 200 $\times$ 200 μm^2. These squares were written by successively increasing the exposure time in each square. The values of ion fluence varied from 0.15$\times$ 10^{14} to 3.75$\times$ 10^{14} ions cm^{-2}.
After exposure to the ion beam, the sample was masked on one side, see fig. 4.1b. Then, the glass sample was submerged in the etching solution (6.0% HF and 0.5% HCl) for 2 min, next, it was rinsed in DI water and dried with N_2 gas and finally its profile was measured. After measuring its profile, the same sample was masked and again submerged in the etching solution for two minutes. The same steps were

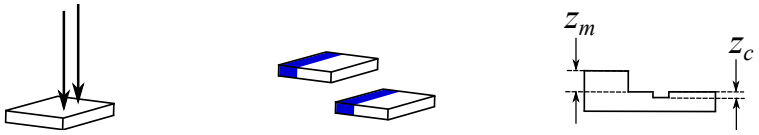

(a) (b) (c)

Figure 4.1: (a) Direct writing on the surface of the glass (b) After exposure, the unexposed area of the substrate is covered with an adhesive tape and (c) shows a representation of the resulting profile for an etched sample.

repeated until the total etching time reached 20 min.

The resulting etched depths were measured with the profilometer. One side of the glass is not exposed nor etched (z_m), and there is the effective etched depth, which is measured as the difference from the etched unexposed and etched exposed (z_c). Figure 4.1c depicts the resulting profile after etching.

4.3.2 Simple pattern lithography

Figure 4.2 represent the steps followed to obtain a microfluidic device by using MeV ion beam lithography, wet etching and thermal bonding. A channel was written on the glass with approximately $2\times\ 10^{14}$ ions cm^{-2}. Then it was etched in the HF:HCl solution. When the microchannel had been etched, the glass sample was bonded to a coverslip.

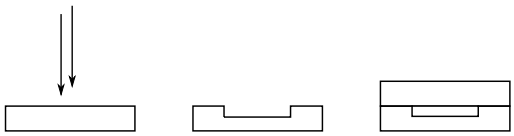

(a) (b) (c)

Figure 4.2: Schematic of ion beam lithography procedure. Glass sample is represented as a transverse section of the chip. In (a) direct writing over the glass substrate by $^{16}O^{3+}$ ions. (b) Representation of the profile resulting from HF etching of the exposed area, and (c) shows a thermally bonded sample.

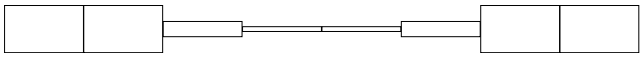

Figure 4.3: Design pattern for MeV lithography. The length of each rectangle is 500 μm and it is 40 μm wide in its thinner section.

A succession of exposed rectangles of different sizes will yield a simple microchannel on the surface of the sample. Fig 4.3 represents the channel to be exposed. Each rectangular exposure is 500 μm long, and the thickness of each rectangle varied from 300 μm, 100 μm and 40 μm, as shown in fig 4.3. The middle section is intentionally thinner because it represents the sector for analyte detection.

After direct writing of the microchannel on the glass, the samples were etched in HF:HCl 6.0:0.5 % v/v for 20 min. Then they were rinsed in DI water for 5 min and dried with N_2 gas. The patterns were visualized under a microscope, then it was measured with the profilometer to determine its depth and examine its surface roughness.

With the aid of an optical microscope the beginning and the end of the channel were visualized and their positions were marked. Then, with a high speed rotary tool equipped with a diamond tip (d=1 mm) two holes were drilled at these positions to provide access to the channel. Then the samples were cleaned with soap and water to remove the debris released from drilling the holes. After cleaning, annealing at 550 °C of the substrates was performed. Once the samples were clean they were prepared to be thermally bonded in a programmable furnace, see fig. 4.2c.

4.4 Electron beam lithography

Figure 4.4 describes schematically the fabrication steps followed to obtain a microfluidic device in glass by EBL. The samples were prepared from 1 mm thick glass squares. First, 1 mm diameter inlet and outlet holes were drilled through the glass. The holes were separated approximately 4 mm form each other. After drilling the holes, the samples were cleaned with acetone, rinse with IPA and dried in N_2 gas.

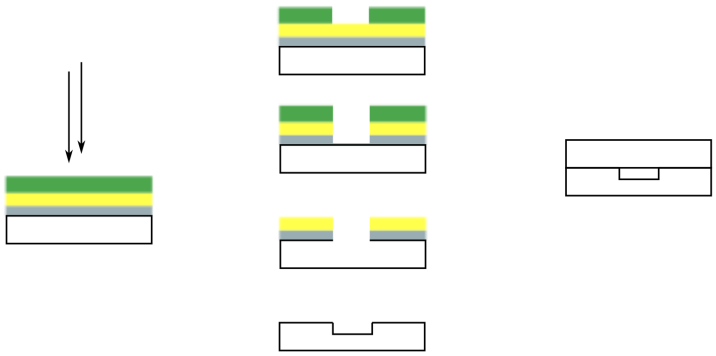

Figure 4.4: Schematic of the procedure used in electron beam lithography. Glass sample is represented by its transverse section. (a) shows a prepared sample which contains a Cr layer (gray color), Au layer (yellow color) and PMMA (green color) on top of the surface. The positive resist is exposed selectively to an electron beam. In (b) there are the results of the steps of several developing and etching procedures that are needed to reach and etch the glass surface. (c) Displays the bonded sample.

A metal mask was deposited on the surface of the samples by using a Balzers BAE 250T high vacuum electron beam evaporator. With a deposition rate of approximately 1.5 Å/s a 5 nm Cr layer and a 100 nm Au layer were added to the surface of the glass.

Commercial Microchem positive resist was used for patterning. Polymethylmethacrylate dissolved in anisole (PMMA A 4%) with a molecular weight of 950 u was spin coated at 2000 rpm for 45 s. After spinning, the sample was baked on a hot plate at 160°C for 3 min which results in a ∼300 nm thick PMMA layer, the resulting layers and the glass are shown as a cross-section in fig. 4.4(a) .

The patterns were exposed with Raith e-line electron beam writer and Elphy Quantum 4.0 lithography software. With an acceleration voltage of 20 kV the pattern shown in fig 4.5 was directly written on the resist. The alignment system within the computer allows to write the pattern precisely between the previously drilled holes, assuring that they are linked through the microchannel.

To transfer the pattern into the glass substrate, first the PMMA was developed in MIBK(methylisobutylketone):IPA with a ratio of 1:3 for 1 min, then rinsed in IPA

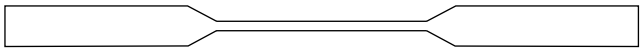

Figure 4.5: Design pattern for electron beam lithography. The thickness is 600 μm in the wider section and 100 μm in the thinner section.

and dried in nitrogen flow. This step reveals the exposed section in the mask layer beneath the PMMA. Then the sample was etched for 3 min in Aqua Regia solution $HCl:HNO_3:H_2O$ with a 3:1:2 ratio to remove the exposed area of Cr and Au. After this procedure, the glass surface to be etched is revealed. Finally, the substrate was immersed into 4 % HF for 40 min without agitation to prevent deterioration of the metal mask. Then it was rinsed in DI water. The remaining Cr/Au layer has to be completely removed by cleaning with Aqua Regia and then ultrasonic cleaning in DI water. These steps can be seen in fig. 4.4b.

The sample was observed under a microscope through the procedure to visualize the integrity of the mask and also to check that the microchannel had transferred to the sample. Then it was measured with the profilometer to determine its depth and visualize its surface the roughness. After the lithographic process was completed, annealing of the substrates was performed and strict cleaning procedures was done.

4.5 Thermal bonding procedures

With the available reported techniques described in section 2.6, the assays for temperature range and different weights were tested. These tests were performed in glass squares without exposure to establish the necessary parameters for bonding glass.

Different cleaning steps that involve the use of acetone, IPA, H_2O_2 and ultrasonic baths in DI water were used. Also, to release the stress in the substrate and to evaporate any surface contaminant, annealing at 550 °C was performed.

Bonding can be improved by increasing the contact in the interface of the glass chip. So in addition to the cleaning procedure and the temperature determination, the effect of the addition of external pressure on the chip was examined by using several

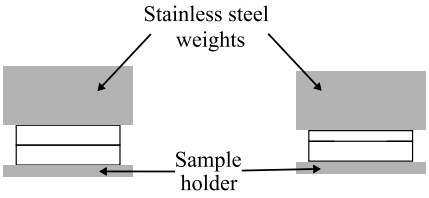

Figure 4.6: *Sandwich* configuration used to test several weights and temperature range to achieve successful bonding between two sodalime glass squares.

stainless steel weights on the top of the bonding glass. Fig. 4.6 shows the transverse section of the configuration used for testing. The trials were performed with 36 g, 73 g, 109 g, or 160 g of steel on top of two glass combinations, two 1 mm thick slides and one slide and one coverslip. This *sandwich* configuration was placed in a furnace oven at different temperatures that vary from 560 to 580 °C.

After several trials for bonding two pieces of glass without exposure were performed, the assays for bonding patterned samples was done. Regardless of the lithographic technique chosen for patterning, this study uses two procedures to bond one piece of glass that contains the lithographic pattern and either a slide or a coverslip cap without patterning.

Glass slides and coverslips were cleaned first with acetone, DI water and later in (∼75 °C) hydrogen peroxide (H_2O_2) solution for 10 min. After cleaning the samples, they were activated in ammonium hydroxide at 50 °C for 30 min. Then they were dried on the hot plate (∼75 °C) and subsequently placed in contact with each other with pressure applied on top by the addition of 73 g weight. All this configuration was placed into a programmable furnace (GERO Hochtemperaturöfen GmbH & Co.) at 550 °C during 5 h with ramp rate 1 °C/min and cold down 1 °C/min, procedure previously reported by Mao and Han [42].

The other bonding procedure includes a pre-cleaning step by using acetone and IPA. Then, ultrasonic cleaning in DI water for 30 min with water changed every 3 min. Later, the samples were placed in H_2O_2 heated to approximately 75 °C for 30 min. Immediately after, the samples were placed in contact with each other. When they were together, they were placed on the hot plate at 75 °C with the holes of the

chip facing up until they were visibly dried. Following the procedure presented by Chen et al. [45]. Once they were dried 73 g weight was added on the top to make a sandwich configuration. Finally this was placed into the programmable furnace under the same ramp procedure mentioned before.

4.6 Raman spectroscopy measurements

A solution containing HipCO tubes (Carbon Nanotechnologies Incorporated) in 1% SDBS aqueous solution were used as the analyte for detection of carbon nanotubes in a Raman Spectroscopy system. The Raman spectroscopy setup is equipped with a laser of 532 nm (Alphalas Monolas 532-100-SM) with a power of 11.5 mW. The system contains a spectrometer Acton SpectraPro 2500i and it is used with 600 1/mm grating.

The sample holder is on a piezoelectric stage that allows accurate movement of the sample controlled by a computer. Fig. 4.7 depicts the glass microfluidic chip on the sample holder. The HipCO solution was added into the microchannel by adding a

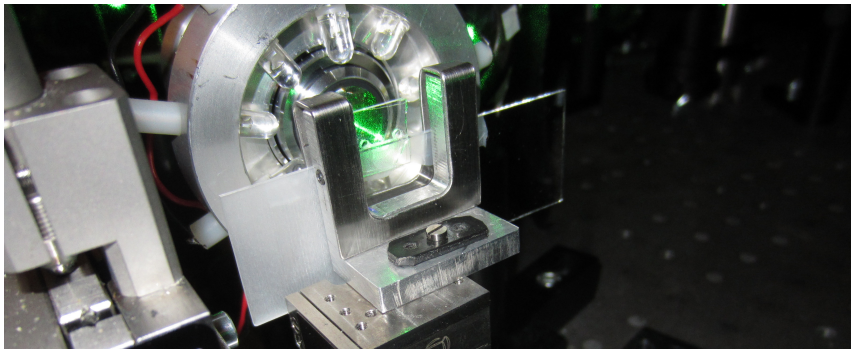

Figure 4.7: Microfluidic chip holder in the Raman spectroscopy setup. The sample holder shows the microfluidic device attached to a microscope slide, only the inlet and outlet holes are visible in the microfluidic device. The green laser is focused on the microchannel that lies between the inlet and outlet holes. Behind the sample holder there is a microscope objective lens surrounded by LED lights.

drop of the solution with a syringe on the inlet. This drop quickly fills the channel by capillary forces. Immediately after adding the solution the microfluidic device is placed on the sample holder.

Then, the laser is focused into the microchannel. To focus the laser in the microchannel, a microscope objective (Nikon LU Plan, ELWD 50 x / 0.55 B, WD 10.1) was used, see fig. 4.7. By adjusting the focus, the focal plane of the laser will correspond to the inside of the microchannel. This steps were visualized in the computer screen.

Prior to the measurements, the backscattering signal was collected for 1 s and recorded. Then, the Raman spectra were acquired using Andor Solis 4.14.30001.0 software. The spectra were measured as 10 s single scan acquisitions in different positions.

5 Results and Discussion

This chapter gives the details of the measurements obtained through this study. The fabrication protocols are discussed and compared. In addition analysis and interpretation of the results is performed.
The best protocols for the fabrication techniques and their restrictions are presented. Moreover, this chapter includes several recommendations that can be pursued to enhance the characteristics of glass microfluidic devices.

5.1 Characteristics of wet etching of sodalime glass

The etch rate of sodalime glass was calibrated by controlling the time that glass is submerged in the HF. Fig. 5.1 (next page) presents the measured profile of the etched channel. The etching time for this channel was 20 min and its dimension are 1 mm in width and $\sim$ 28 μm deep.
A characteristic present in channels made by wet etching is that the bottom of the channel is rounded, see fig. 5.1. This feature is present because HF is an isotropic etchant [33]. The same behavior has been previously reported by Iliescu et al. [10, 34] for pyrex glass and for sodalime glass see Rodriguez et al. [8].
Fig. 5.1 shows that the surface roughness at the sides of the channel is low , therefore there is no leaking of HF between the tape and the glass. The polymer adhesive tape used as a protective mask works very efficiently because it allows selective etching of the glass. The tape presents good adhesion to the surface. Also, the addition and removal of the tape yields no surface modification of the glass substrate. As a consequence, the sections that were masked remain unaltered.
The resulting etch depth was related to the immersion time. The correlation between etch depth and etching time for each solution is shown in fig. 5.2 (next page). The

etch rate for the solutions yields 0.572 µm/min for 4% v/v HF and for the mixed solution of HF:HCl it is 1.0754 µm/min.

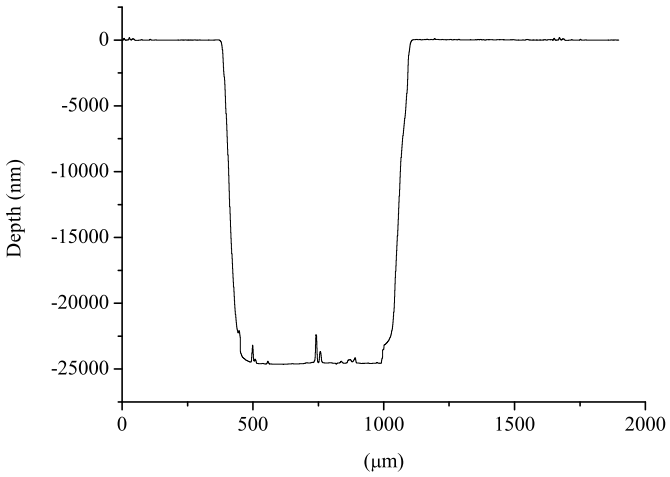

Figure 5.1: Profile of the channel made by wet etching during 20 min in the HF:HCl solution.

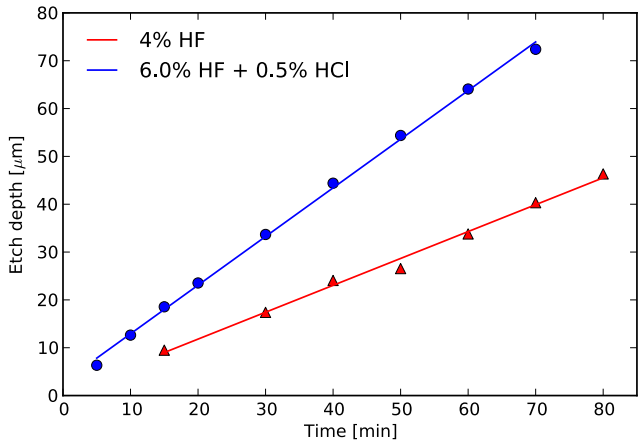

Figure 5.2: Etch depth as a function of time for 4% v/v HF and 6:0.5% v/v HF:HCl of sodalime glass

5.2 MeV ion beam lithography

5.2.1 Characteristics of $^{16}O^{3+}$ ion beam irradiations on sodalime glass

Figure 5.3 shows the profile of the exposed glass sample. The pattern was made from writing 200 $\times$ 200 μm^2 squares on the glass by increasing their exposure time. The measured length of the squares is about 170 μm. This disparity comes from a calibration deviation in the PPAL system at the time of exposure. The thickness of the patterns does not affect the measurement of the depth as a function of the ion fluence.

Ion fluence is one of the main parameters that should be defined to obtain a desired pattern with the required depth into a substrate. For the ion fluence used, the etched depth increases as the ion fluence increases. Also, the etched profile of the squares present rectangular cross-sections, see fig. 5.3.

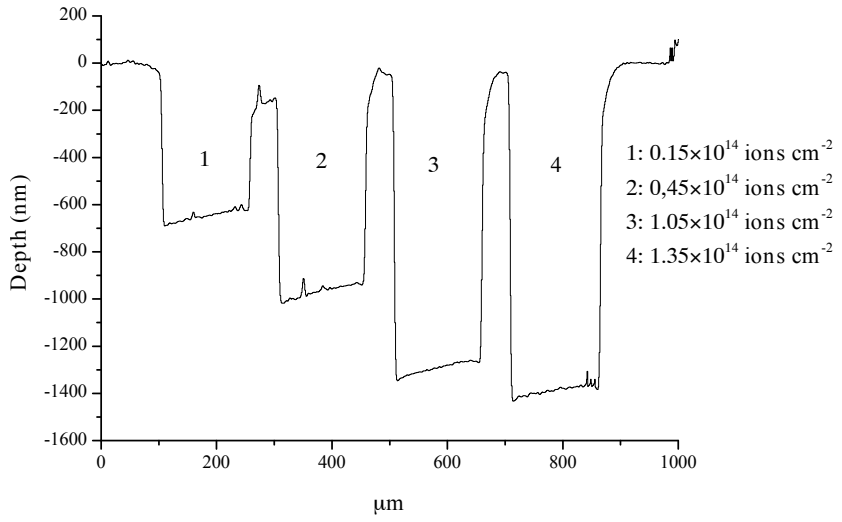

Figure 5.3: Profile of the squares patterned with increasing values of fluence from 0.15 $\times$ 10^{14} to 1.35 $\times$ 10^{14} ions cm^{-2}. Each square is denoted by a number that corresponds to the fluence used.

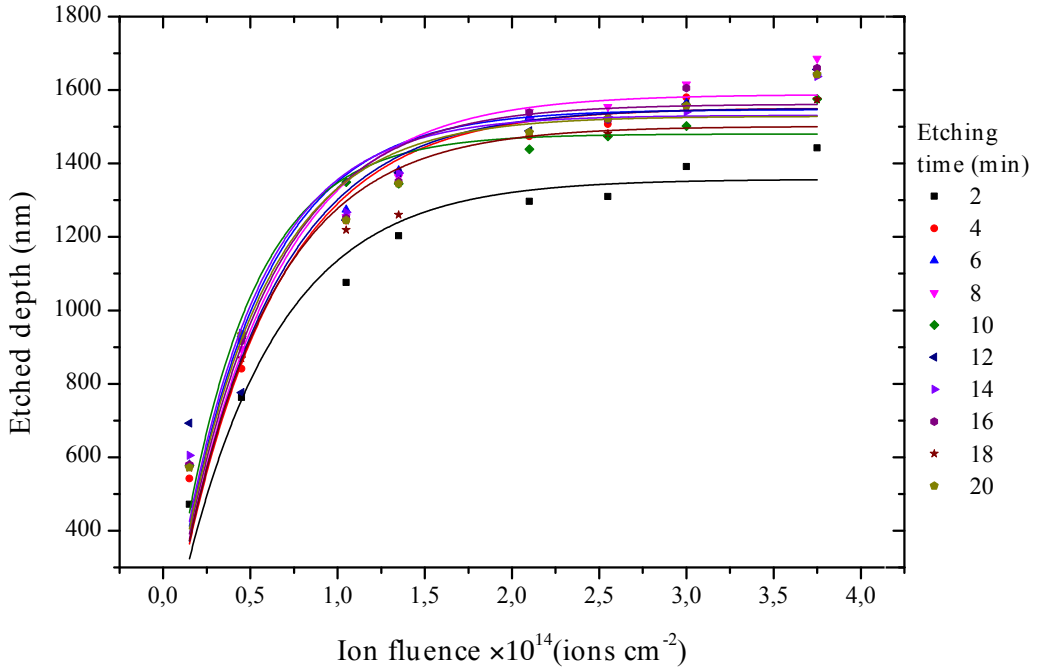

Figure 5.4: Experimental etch depth of 200 × 200 μm^2 squares as a function of increasing $^{16}O^{3+}$ ion fluence. The samples were etched in 6.0% HF and 0.5% HCl for different times. Each point represents the depth of one square.

The experimental depth of a pattern written in glass is also dependent on the etching time. Figure 5.4 depicts the relationship of the etched depth as a function of the ion fluence for different etching times. When the ion fluence is $\geq 1.5\times10^{14}$ ions cm^{-2} the etch depth reaches its constant value.

The behavior in fig. 5.4 is represented by the exponential model

$$z = A \cdot (1 - e^{-k\cdot\phi}), \tag{5.1}$$

where z represents the effective etch depth in nm and A is the amplitude or maximum etched depth in nm. k is known as the exponential etch constant in cm^2/ions, and ϕ is ion fluence in ions cm^{-2}. Equation 5.1 is suitable to describe the behavior because it represents the physical phenomena in accordance to the initial conditions of the experiment. For instance, for $\phi = 0$, $z = 0$. This condition indicates that if

Table 5.1: Fitted parameters for the increasing values of fluence in sodalime glass. These parameters correspond to fig. 5.4

Time	**Amplitude**	**Exponential constant**	**Time**	**Amplitude**	**Exponential constant**
t	***A***	***k***	**t**	***A***	***k***
min	**nm**	**cm^2/ions** $(\times 10^{-14})$	**min**	**nm**	**cm^2/ions** $(\times 10^{-14})$
2	1375	1.81	12	1550	1.82
4	1551	1.78	14	1531	2.16
6	1546	2.06	16	1561	1.92
8	1588	1.80	18	1501	1.90
10	1480	2.31	20	1528	2.05

there is no irradiation of the sample there is no exposed etched depth. Also, when $\phi \to \infty$; $e^{-k\cdot\phi} \to 0$ and therefore $z \to A$. So it is reasonable to approximate the behavior of the oxygen ions into sodalime glass with eqn. 5.1. The same exponential behavior has been reported by Momota et al. [28] for exposure of Si with Ar beam and for irradiating silica with oxygen ions by Puttaraksa et al. [27].

Table 5.1 presents the fitted parameters for eqn. 5.1 of the amplitude and exponential constant for the different etching times. Results show fluctuations $\leq$ 100 nm in the amplitude from 4 to 20 min, therefore the 6.8 MeV $^{16}O^{3+}$ ions have reached the experimental amplitude in sodalime glass. The amplitude yields 1.5 μm when $\geq 1.5\times10^{14}$ ions cm^{-2} is used.

The exponential behavior obtained through the measurements implies that to obtain a constant etched depth during MeV lithographic procedure the fluence has to remain higher than 1.5×10^{14} ions cm^{-2}. Also, with a fluence larger than 1.5×10^{14} ions cm^{-2} the experiment will not be sensitive to big changes of ion current in the accelerator or temperature variations.

5.2.2 Wet etching behavior of exposed sodalime glass

When a sample has been exposed with the same ion fluence, the depth that can be achieved is dependent on the etching time. For instance, the depth of the exposed area (3×10^{14} ions cm^{-2}) increases 0.22 μm from 2 to 8 min, see fig. 5.4 on page 31. The experimental behavior for the effective etched depth as a function of time for the different ion fluence used is shown in fig. 5.5.

There an increase in the effective etch depth in the first time interval for all ion fluence utilized. For example, from 2 to 4 min the change in depth is 0.18 μm (for 3.00 $\times 10^{14}$ ions cm^{-2}). After 6 min of etching time, the differences in the etched depth are small ($\sim$ 0.03 μm). Results suggest that when exposed glass has been etched, a maximum effective etched depth (z_c) is reached at a threshold time for each ion fluence.

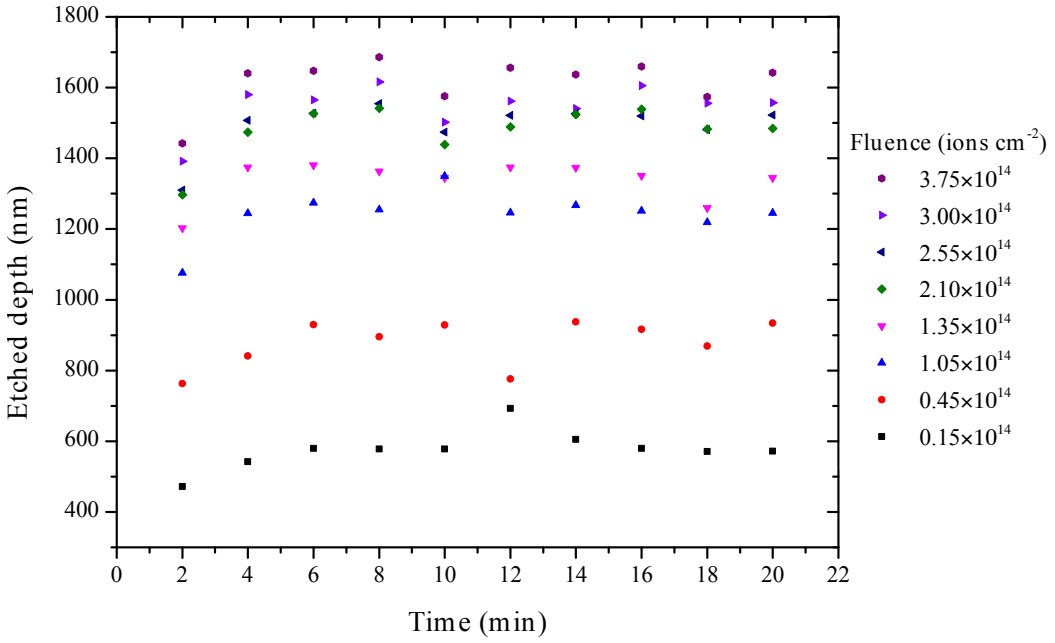

Figure 5.5: Effective etch depth z_c as a function of the etching time for different ion fluence values.

Table 5.2: Measured depth for an etched square exposed to ion fluence of 3.00 $\times 10^{14}$ ions cm^{-2}

Etching time **min**	**Height of masked surface** z_m **(µm)**	**Depth of exposed area** z_c **(µm)**	**Total etched path** $z_m + z_c$ **(µm)**
2	2.42	1.39	3.81
4	4.33	1.56	5.89
8	10.71	1.59	12,30
16	21.47	1.60	23,07

To obtain the experimental penetration range of the ions it is necessary to consider the etched exposed and unexposed depth. Table 5.2 shows the height of the masked surface (z_m), the depth of the etched exposed area (z_c) and the total etched distance for selected etching times. For 2 min the total etched depth does not reach the theoretical penetration range of 4.8 µm obtained by SRIM, and for 4 min the total etched depth exceeds the theoretical penetration range by 1.1 µm.

The proposed model in fig. 2.4 in section 2.5, coincides to the experimental behavior of exposed and etched sodalime glass. The experimental threshold etching time t_2 for exposed glass relies between 2 and 4 min. This results show that the experimental effective etched depth of 1.5 µm have been achieved when using 4 min of etching time.

A reduction in etching time is a desirable characteristic of fabrication of microfluidic devices [36]. Therefore obtaining the precise threshold etching time value is important to reduce manufacturing time, reduce surface roughness and enhance further bonding procedures. By the procedures used through this study it was possible to determine that less than 4 min will be necessary to achieve the maximum penetration depth of 6.8 MeV $^{16}O^{3+}$ ions in sodalime substrate.

Another approach to control the etching rate of exposed sodalime glass relies in lowering the concentration of HF and performing a similar procedure. This way the etch rate will be reduced and the etch depth could be controlled more accurately. If this procedure is utilized the etching threshold time can be determined accurately.

5.2.3 Microfluidic device with microchannel made by ion beam lithography

When the exposure and etching parameters have been explored, a microchannel was patterned and etched in glass. Figure 5.6 presents the profile of the etched microchannel in its thinnest section. The roughness after etching of the exposed and unexposed glass is low. The effective etched depth of the channel is 1.6 µm which is the expected experimental depth according to the amplitude values obtained in table 5.1.

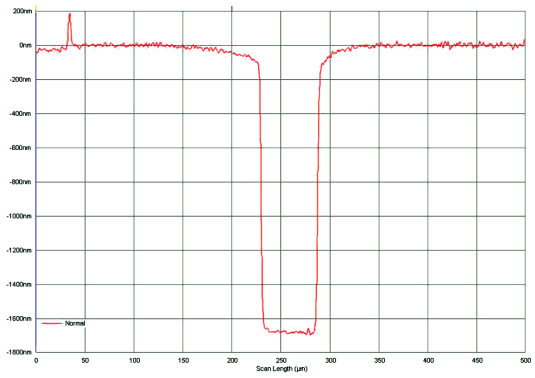

Figure 5.6: Profile of the thinner section of the a microchannel made by MeV lithography.

Bonding of the microfluidic chip was done by cleaning and activating the glass surfaces with H_2O_2, then they were held at a maximum temperature of 550°C in a sandwich configuration with a 73 g steel weight on top. In figure 5.7 there is a micrograph of the exposed, etched and bonded channel.

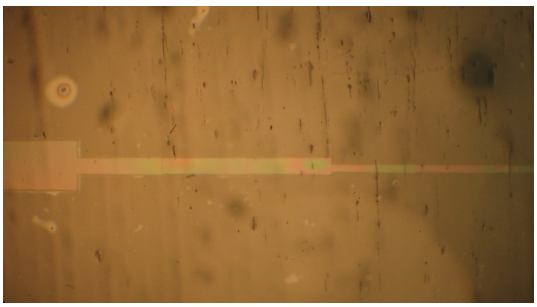

Figure 5.7: Enclosed microchannel made by MeV lithography. Picture shows the channel sections of 300, 100 and 50 µm wide from left to right.

Inside the microchannel Newton rings are visible. Light is reflected from both sides of the thin air gap within the microchannel and this interference give rise to the colored pattern. These indicate that the area of the channel is not bonded. Contrary to the areas next to it, in which there are no Newton rings visible. Some of the ridges that are visible on the micrograph come from the weights used during bonding procedure.
Through the MeV ion beam lithography technique it was possible to pattern a shallow pattern ($\sim$1.6 μm) in a glass substrate. Also by using thermal bonding it was possible to preserve the characteristics and properties of the glass. The microfluidic chip obtained is completely transparent which make it suitable for optical detection system.

5.3 Electron beam lithography

Electron beam lithography can be used to write a pattern on glass indirectly. The pattern has to be transferred from the PMMA through the Au/Cr protective layers into the glass substrate. At first, when the glass was submerged in the 4% HF solution the protection layer was unmodified, but after $\sim$5 min some bubbles started to appear on the surface of the Au/Cr layer. These bubbles indicate that the HF has reached the protected section of the glass by leaking into the interface between the glass substrate and the protection layer. Otherwise, the layer should remain flat.
If the substrate is dirty, due to particle contamination, the adhesion of Cr layer and the glass surface is poor. For this reason there could be leaking of HF. Moreover, the reported values for Au/Cr mask layers are thicker [37]. Nevertheless, since the HF concentration used in this experiment was low, the protective mask was kept thin.
Figure 5.8 shows that there is a difference in the surface quality between the bottom of the channel and the masked areas. There is an increase in the roughness of the masked areas, specifically on the right side of the microchannel in fig. 5.8 (next page). This depression indicates that the HF reached the interface between the protection layer and the glass.

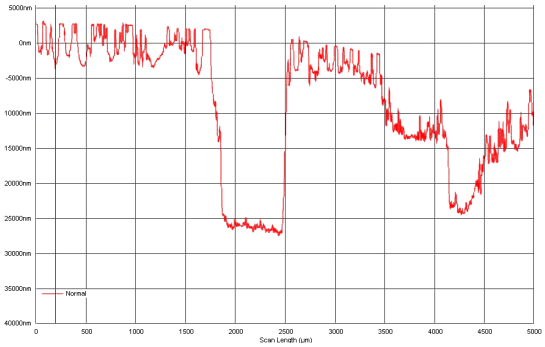

Figure 5.8: Measured profile of a microchannel made in sodalime glass by electron beam lithography.

The etched microchannel was capped with one coverslip and successfully bonded by activating its surface with H_2O_2. Also, a maximum temperature of 550°C with a 73 g mass yielded a bonded microfluidic chip despite the increase in the surface roughness.

Figure 5.9 shows the enclosed channel filled with water. Some stripes are visible on the surface. These correspond to ridges transferred from the stainless steel weights to the surface of the glass during the bonding step. To prevent this surface modification, thermal bonding in vacuum without additional pressure can be performed. Also rigorous polishing of the metal weights can improve the surface quality.

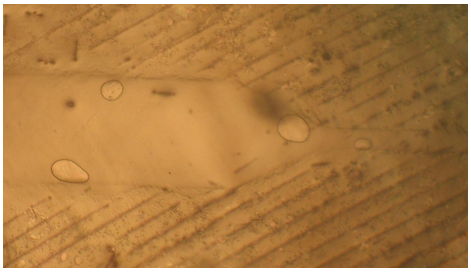

Figure 5.9: Simple microfluidic channel made by electron beam lithography combined with wet etching. The channel is enclosed with a coverslip. Its dimensions are 600 µm and 100 µm on the thicker and thinner section respectively. The channel is filled with water and some air bubbles are visible.

5.4 Comparison of the lithographic techniques

Two lithographic techniques were tested to produce a microfluidic channel in glass. Results show that both of them are suitable for fabrication of microchannels, however the characteristics of the fabrication of the device and the resulting microfluidic chip vary.

The treatment of the sample prior to the lithographic procedure is different. For instance, IBL allows direct exposure of the substrate in which no mask or strict cleaning of the sample is needed. And for EBL one of the most important details is the deposition of the protection films before exposure because further processing steps depend on having proper adhesion between the etch mask and the substrate. It is important that while etching, the HF does not leak to the interface because this results in an irregular profile that will reduce the bonding success. Annealing and pre-treatment of the surface may improve the adhesion of the mask layer

The depths that can be achieved with the two techniques differ. With 6.8 MeV oxygen ion beam lithography (IBL), theoretically 4.94 μm deep structures can be reached, but in the experimental depth achieved was 1.6 μm. This is due to the high etch rate of unexposed glass, see table 5.2 on page 34. In contrast, EBL enables deeper channels to be produced in glass. However, different depths will be difficult to achieve because they will require many steps of mask deposition and development in addition to several exposures. The etch depth by EBL depends on the integrity of the mask and when using IBL the etched depth depends on the ion fluence and the etching time. Therefore EBL provides means to obtain deeper microchannels, under the condition that the protective layer withstands the acid.

The profiles of the channels made by IBL and EBL are shown in fig. 5.6 and fig. 5.8 respectively. The bottom of the microchannel is slightly smoother in the channel made by IBL and it has a rectangular cross-sections with straight walls. The microchannel made by EBL shows that the roughness of the unexposed area has considerably increased.

Two techniques have been explored to make a simple microfluidic channel, results

show that both techniques are reproducible and microchannels of with different characteristics can be obtained. The purpose of exploring and comparing these techniques is to improve the fabrication procedure, reduce the manufacturing time and being able to enhance the desired characteristics of the chip.

5.5 Thermal bonding of microfluidic chip

Bonding represents the most challenging step in the fabrication of glass microfluidic device [10, 43, 46]. It is time consuming and requires strict procedures. However, thermal bonding is known to produce permanent and high strength bonds that withstand high pressure. Therefore it is useful for a wide variety of applications.
The most critical detail is cleaning the glass. Any trapped particle in the interface of two glass pieces represents a gap that will reduce the adhesion. These particles could be responsible for leaking of the analyte.
Results show that annealing of the glass at 550 °C and soaking in acetone and IPA removes organic and inorganic contaminants present on the surface. Additionally when performing the procedure it is beneficial to implement ultrasonic agitation in DI-water. These cleaning steps were the most adequate to obtain strong bonds.
An activated glass surface is obtained when the surface is covered by hydroxyl groups ($-OH$). These groups are highly reactive and will allow oxygen bonds to form between the two pieces of glass when they are held in direct contact to each other [42, 45].
When glass samples have been activated with H_2O_2 they exhibited slight linking to each other when they were pressed together. For instance, the samples could be moved gently with a tweezer and both pieces of glass will remain together. This indicates the presence of hydrogen bonds and Van der Waals bonds within their interface. The samples activated with NH_4OH displayed less adhesion, therefore it was easier to unbind them. Therefore hot (75°C) H_2O_2 was preferred over NH_4OH for activation of the surface. When weak attachment due to hydrogen bonds is present, the microfluidic chip can undergo thermal bonding and strong permanent binding

most likely will occur.

Results show that 560-570 °C was too low temperature to allow bonding and above 580 °C the substrates melted. Also, this high temperature could damage the microstructures within the glass. In addition to thermal bonding temperature determination, by this procedure it was possible to determine that the weight used will be dependent on the size of the chip and the thickness of the glass in hand.

For 1 cm^2 samples, weights of 73 g provided enough pressure to make stable bonds. Adding more weight, 109g or 160g, resulted in either deterioration of the surface of the chip or collapse of the channels. Whereas less weight, such as 36g, provided weak bonds. Under this condition the bonded chip lacked adhesion to comprise liquid inside of the microchannel.

When bonding sodalime glass of different thickness, for example slide and coverslip, it is very important to avoid abrupt temperature changes $\Delta T = 30$ °C. If there is a fast change in the temperature the coverslip will become cold faster and the difference in stress will result in cracks that induce leaking and eventually the bonded chip will break. It is beneficial to utilize annealing of the glass before the thermal bonding procedure to relieve stress.

The furnace should keep a constant temperature to ensure that both glasses, despite their thickness maintain a uniform temperature between the two pieces. When two pieces of glass of the same thickness are bonded, cracks due to distinct stress were rare.

The bonding procedure used in this study found to be appropriate to bond glass surfaces that are either patterned pieces or flat. The bonding method successfully attached microchannels that vary from 600, 100, 50 μm wide and 1.8 to 25 μm deep. Also it is suitable for bonding samples with different surface roughness.

Glass-glass direct bonding grants the final device some advantages. The microfluidic chip will be composed of the same material, and therefore the properties of the substrate are identical in all its internal walls. For example, liquid will spread through the channel with the same velocity profile because the contact angle is the same in all directions. Also, the surface charge is equal therefore electrokinetic ex-

periments can be performed and direct bonding provides the final device with homogeneity in the inside walls of the microchannel.

5.6 Raman spectroscopy measurements from the microfluidic device

The fabricated microfluidic device was tested on a Raman spectroscopy system. The microchannel with dimensions 1.8 μm deep and 50 μm wide was filled with HipCO solution for this test. The measurement setup used has a small signal collection area. This is very convenient because it avoids encountering the imperfections on the surface of the microfluidic chip, for example the ridges that were transferred when bonding.

Fig. 5.10 shows the measured Raman spectrum. The RBM mode and G-Band peaks characteristic of carbon nanotubes are visible. The measurement conditions were maintained but after one minute had passed there was no signal recollection from the HipCO solution. Therefore, results suggest that the signal depends strongly on the nanotube movement and distribution inside the microchannel.

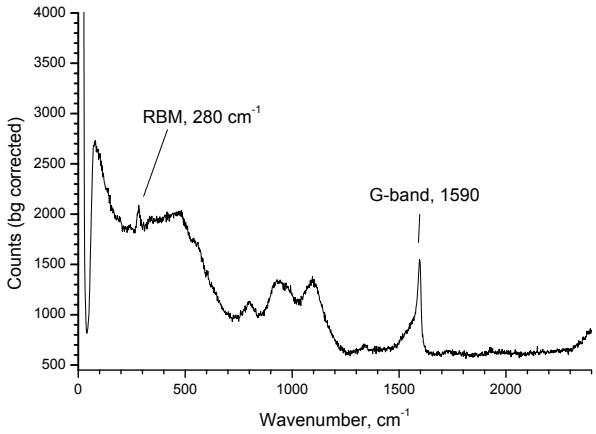

Figure 5.10: Raman spectra collected from HipCO carbon nanotubes in 1.8 μm deep microchannel for 10 s

The HipCO solution often yields SWNT of various radii, in average from 0.8 to 1.2

nm [54]. According to eqn. 3.4, the diameter of the measured nanotubes is 0.83 nm correspondingly to the HipCO solution.

The microfluidic device achieved by this study is suitable for optical measurements because it provides a strong Raman signal. The presence of a cap coverslip is beneficial because it is thinner than the microscope slide and therefore provides less background spectra signal.

This simple channel can be used for mapping spatial concentrations or probe chemical compounds. Detection of the carbon nanotubes in this regime is suitable for applications of sorting and purification. The addition of controlled movement of the solution as pressure driven by a pump syringe will be desirable. Finally, further research can be performed by functionalizing the carbon nanotubes.

6 Conclusion

There are several factors that will affect the performance and uses of a microfluidic device. The composition of the substrate, the fabrication method, the detection system and the analyte are all related and depend on each other. This research dealt with the optimization of fabrication processes that involved the patterning, wet etching, bonding and probing of compounds in a glass microfluidic channel.

Detailed information on the use of two lithographic techniques, ion beam lithography and electron beam lithography, for manufacturing a channel within a glass substrate was obtained. The etching characteristics were obtained for 6.8 MeV $^{16}O^{3+}$ exposed and unexposed sodalime glass. Moreover, the cleaning procedures, the bonding temperature and pressure parameters for thermal bonding were acquired to successfully bond sodalime glass.

As the main outcome of this study a simple microfluidic chip with a microchannel 50 μm wide and 1.6 μm deep suitable for optical measurements was fabricated. The microfluidic device obtained through this research is functional in an optical detection system. It was tested in an optical spectroscopy system by measuring the Raman spectrum from carbon nanotubes traveling within the microchannel. The microfluidic device showed positive detection of carbon nanotubes within the channel intermittently.

Glass based microfluidic devices offer many opportunities in optical detection methods that are yet to be discovered. These devices promise new possibilities and opportunities related to controlled fluid movement. Complex channel designs may be used in the future for mixing and sorting which represent challenging opportunities and new emerging experiments.

Bibliography

[1] G. S. Fiorini and D. T. Chiu. Disposable microfluidic devices: fabrication, function, and application. *Biotechniques*, 38(3):429–46, 2005.

[2] G. M. Whitesides and A. D. Stroock. Flexible methods for microfluidics. *Physics Today*, 54(6):42–48, 2001.

[3] X. L. Zhang and S. J. Haswell. Materials matter in microfluidic devices. *Mrs Bulletin*, 31(2):95–99, 2006.

[4] F. Sarrazin, J.-B. Salmon, D. Talaga, and L. Servant. Chemical reaction imaging within microfluidic devices using confocal Raman spectroscopy: The case of water and deuterium oxide as a model system. *Analytical Chemistry*, 80(5):1689–1695, 2008.

[5] Z. Wang, W. Wang, W. Wang, Li. Xu, G. Chen, and F. Fu. Separation and determination of β casomorphins by using glass microfluidic chip electrophoresis together with laser-induced fluorescence detection. *Journal of separation science*, 34(2):196–201, 2011.

[6] Ch. Chou, N. Jing, H. Yamaguchi, P. Tsou, H. Lee, C. Chen, Yi. Wang, S. Hong, C. Su, J. Kameoka, and M. Hung. Rapid detection of two-protein interaction with a single fluorophore by using a microfluidic device. *Analyst*, 135:2907–2912, 2010.

[7] J. B. Salmon, A. Ajdari, P. Tabeling, L. Servant, D. Talaga, and M. Joanicot. In situ Raman imaging of interdiffusion in a microchannel. *Applied Physics Letters*, 86(9):094106, 2005.

[8] I. Rodriguez, P. Spicar-Mihalic, C. L. Kuyper, G. S. Fiorini, and D. T. Chiu. Rapid

prototyping of glass microchannels. *Analytica Chimica Acta*, 496(1-2):205–215, 2003.

[9] P. Zhang, G. Londe, J. Sung, E. Johnson, M. Lee, and H. J. Cho. Microlens fabrication using an etched glass master. *Microsystem Technologies-Micro-And Nanosystems-Information Storage and Processing Systems*, 13(3-4):339–342, 2007.

[10] C. Iliescu, H. Taylor, M. Avram, J. Miao, and S. Franssila. A practical guide for the fabrication of microfluidic devices using glass and silicon. *Biomicrofluidics*, 6(1):16505–1650516, 2012.

[11] J. Zhou, A. V. Ellis, and N. H. Voelcker. Recent developments in PDMS surface modification for microfluidic devices. *Electrophoresis*, 31(1):2–16, 2010.

[12] Y. Chen, L. Zhang, and G. Chen. Fabrication, modification, and application of poly(methyl-methacrylate) microfluidic chips. *Electrophoresis*, 29(9):1801–1814, 2008.

[13] H. J. Whitlow, L. Rojas, R. Norarat, M. Napari, and H. Kivistö. (In press). Lithographic fabrication of soda-lime glass based microfluidics. In *Elsevier Editorial System for NIMB Proceedings*, 2012.

[14] J. R. SooHoo, J. K. Herr, J. M. Ramsey, and G. M. Walker. Microfluidic cytometer for the characterization of cell lysis. *Analytical Chemistry*, 84(5):2195–2201, 2012.

[15] D. Schafer, E. A. Gibson, E. A .and Salim, A. E. Palmer, R. Jimenez, and J. Squier. Microfluidic cell counter with embedded optical fibers fabricated by femtosecond laser ablation and anodic bonding. *Optics Express*, 17:6068–73, 2009.

[16] Z. Jia, Q. Fang, and Z. Fang. Bonding of glass microfluidic chips at room temperatures. *Analytical Chemistry*, 76(18):5597–5602, 2004.

[17] Z. D. Sandlin, M. Shou, J. G. Shackman, and R. T. Kennedy. Microfluidic electrophoresis chip coupled to microdialysis for in vivo monitoring of amino acid neurotransmitters. *Analytical Chemistry*, 77(23):7702–7708, 2005.

[18] F. E. Regnier, B. He, S. Lin, and J. Busse. Chromatography and electrophoresis on chips: critical elements of future integrated, microfluidic analytical systems for life science. *Trends in Biotechnology*, 17(3):101 – 106, 1999.

[19] L. Cheng and H. Chang. Microscale pH regulation by splitting water. *Biomicrofluidics*, 5(4):46502–465028, 2011.

[20] C. Yi, Q. Zhang, C. Li, J. Yang, J. Zhao, and M. Yang. Optical and electrochemical detection techniques for cell-based microfluidic systems. *Analytical and Bioanalytical Chemistry*, 384:1259–1268, 2006.

[21] N. Puttaraksa. *Development of MeV ion beam lithography technique for microfluidic applications*. PhD thesis, University of Jyväskylä, May 2011.

[22] S. Kondapalli, J. T. Connelly, A. J. Baeumner, and B. J. Kirby. Integrated microfluidic preconcentrator and immunobiosensor. *Microfluidics and Nanofluidics*, 11(5):537–544, 2011.

[23] J. F. Ziegler, M. D. Ziegler, and J. P. Biersack. Srim – the stopping and range of ions in matter 2010. *Nuclear Instruments and Methods in Physics Research Section B: Beam Interactions with Materials and Atoms*, 268:1818 – 1823, 2010. 19th International Conference on Ion Beam Analysis.

[24] D. K. Avasthi and G. K. Mehta. *Swift Heavy Ions for Materials Engineering and Nanostructuring*, pages 47–49. Springer Series in Materials Science. Springer, 2011.

[25] F. Watt, A. A. Bettiol, J. A. Van Kan, E. J. Teo, and M. B. H. Breese. Ion beam lithography and nanofabrication: A review. *International Journal of Nanoscience*, 4(3):269–286, 2005.

[26] A. Razpet, A. Johansson, G. Possnert, M. Skupinski, K. Hjort, and A. Hallen. Fabrication of high-density ordered nanoarrays in silicon dioxide by MeV ion track lithography. *Journal of Applied Physics*, 97(4):044310, 2005.

[27] N. Puttaraksa, M. Napari, O. Chienthavorn, R. Norarat, T. Sajavaara, M. Laitinen, S. Singkarat, and H. J. Whitlow. Direct writing of channels for microfluidic in silica by MeV ion beam lithography. *Advanced Materials Research*, 254: 132–135, 2011.

[28] S. Momota, Y. Nojiri, J. Taniguchi, I. Miyarnoto, N Morita, and N. Kawasegi. Highly charged ion beam applied to lithography technique (Invited). *Review of Scientific Instruments*, 79(2):02C302–1 – 02C302–4, 2008.

[29] S. Gorelick. *MeV ion beam lithography of high aspect ratio structures with a focused or aperture-shaped beam for applications in biomedical studies and microfluidics*. PhD thesis, University of Jyväskylä, September, 2008.

[30] N. Puttaraksa, S. Gorelick, T. Sajavaara, M. Laitinen, S. Singkarat, and H.J. Whitlow. Programmable proximity aperture lithography with mev ion beams. *Journal of Vacuum Science Technology B: Microelectronics and Nanometer Structures*, 26:1732, 2008.

[31] K. A. Addae-Mensah, Z. Wang, H. Parsa, S. Y. Chin, T. Laksanasopin, and S. K. Sia. *Fundamentals of Microfluidics Devices*, pages 1–38. John Wiley & Sons, Inc., 2010.

[32] A. Beaumont, C. Dubuc, J. Beauvais, and D. Drouin. Direct-write electron beam lithography in silicon dioxide at low energy. *Journal of Vacuum Science & Technology B*, 28(5):940–945, 2010.

[33] G. A. C. M. Spierings. Wet chemical etching of silicate glasses in hydrofluoric acid based solutions. *Journal of Materials Science*, 28(23):6261–6273, 1993.

[34] C. Iliescu, Francis E. H. Tay, and J. Miao. Strategies in deep wet etching of pyrex glass. *Sensors and Actuators A-Physical*, 133(2):395–400, 2007.

[35] C. Iliescu, B. Chen, and J. Miao. On the wet etching of pyrex glass. *Sensors and Actuators A-Physical*, 143(1):154–161, 2008.

[36] C. Iliescu and F. E. Tay. Wet etching of glass. In *Semiconductor Conference, 2005. CAS 2005 Proceedings. 2005 International*, volume 1, pages 35 – 44, 2005.

[37] Y. Mourzina, A. Steffen, and A. Offenhausser. The evaporated metal masks for chemical glass etching for biomems. *Microsystem Technologies-Micro-And Nanosystems-Information Storage and Processing Systems*, 11(2-3):135–140, 2005.

[38] F. E. H. Tay, C. Iliescu, J. Jing, and J. Miao. Defect-free wet etching through pyrex glass using cr/au mask. *Microsystem Technologies*, 12(10-11):935–939, 2006.

[39] A. Deshkovskaya. Ion beam-stimulated processes in glasses. *Nuclear Instruments & Methods In Physics Research Section B-Beam Interactions With Materials and Atoms*, 166:511–516, 2000.

[40] K. Liao, N. Yao, and T. Kuo. Sub-60 nm nanofluidic channels fabricated by glass-glass bonding. In *Engineering in Medicine and Biology Society, 2006. EMBS '06. 28th Annual International Conference of the IEEE*, pages 2832 –2835, september 2006.

[41] Y. Lin and Y. Kuo. Fabrication of sub-40 nm nanofluidic channels using thin glass-glass bonding. In *Nano/Micro Engineered and Molecular Systems (NEMS), 2011 IEEE International Conference on*, pages 351 –354, 2011.

[42] P. Mao and J. Han. Fabrication and characterization of 20 nm planar nanofluidic channels by glass-glass and glass-silicon bonding. *Lab on a Chip*, 5:837–844, 2005.

[43] Q. Chen, Q. Chen, and M. Ferraris. Optimization of thermal assisted direct bonding of soda-lime glasses for lab-on chip application. *Microsystem Technologies*, 16(4):527–532, 2010.

[44] B. Renberg, K. Sato, T. Tsukahara, K. Mawatari, and T. Kitamori. Hands on: thermal bonding of nano- and microfluidic chips. *Microchimica Acta*, 166:177–181, 2009.

[45] Q. Chen, Q. Chen, D. Milanese, and M. Ferraris. Thermal assisted direct bonding between structured glasses for lab-on-chip technology. *Microsystem Technologies*, 15(12):1873–1877, 2009.

[46] P. B. Allen and D. T. Chiu. Calcium-assisted glass-to-glass bonding for fabrication of glass microfluidic devices. *Analytical Chemistry*, 80(18):7153–7157, 2008.

[47] E. T. Thostenson, Z. Ren, and T Chou. Advances in the science and technology of carbon nanotubes and their composites: a review. *Composites Science and Technology*, 61(13):1899 – 1912, 2001.

[48] J. M. Schnorr and T. M. Swager. Emerging applications of carbon nanotubes. *Chemistry of Materials*, 23(3):646–657, 2011.

[49] T. W. Ebbesen and P. M. Ajayan. Large-scale synthesis of carbon nanotubes. *Nature*, 358:220–222, 1992.

[50] E. Joselevich, H Dai, J. Liu, Hata K., and A. H. Windle. *Carbon Nanotube Synthesis and Organization*, volume 111 of *Topics in Applied Physics*, pages 101–164. Springer Berlin / Heidelberg, 2008.

[51] J. Yacamán, M. Miki-Yoshida, L. Rendón, and J. G. Santiesteban. Catalytic growth of carbon microtubules with fullerene structure. *Applied Physics Letters*, 62:202–204, 1993.

[52] M. Dresselhaus, A. Jorio, M. Hofmann, G. Dresselhaus, and R. Saito. Perspectives on carbon nanotubes and graphene Raman spectroscopy. *Nano Letters*, 10 (3):751–758, 2010.

[53] A. Jorio, R. Saito, G. Dresselhaus, and M. S. Dresselhaus. Determination of nanotubes properties by Raman spectroscopy. *Philosophical Transactions of the Royal Society A-Mathematical Physical and Engineering Sciences*, 362(1824):2311–2336, 2004.

[54] E. Gregan, S. M. Keogh, T. G. Hedderman, B. McCarthy, G. Farrell, G. Chambers, and H. J. Byrne. Stokes/anti-stokes raman spectroscopy of hipco single-wall carbon nanotubes. *AIP Conference Proceedings*, 633(1):294–297, 2002.